Journal of Magnetic Resonance 197 (2009) 167–175

Contents lists available at ScienceDirect

Journal of Magnetic Resonance

journal homepage: www.elsevier.com/locate/jmr

Dynamic Nuclear Polarization of [1-^{13}C]pyruvic acid at 4.6 tesla

Haukur Jóhannesson *, Sven Macholl, Jan Henrik Ardenkjaer-Larsen

GE Healthcare, Medical Diagnostics, The Grove Centre GC/18, White Lion Road, Bucks, Amersham HP7 9LL, UK

ARTICLE INFO

Article history:
Received 25 June 2008
Revised 15 October 2008
Available online 24 December 2008

ABSTRACT

Dynamic Nuclear Polarization (DNP) of the ^{13}C nucleus has been investigated for [1-^{13}C]pyruvic acid, doped with the trityl radical OX063Me, at 4.64 T and 1.15 K. The dependence of the polarization on microwave frequency, radical concentration and electron saturation was studied. For optimized conditions, a ^{13}C polarization equal to 64 ± 5% was obtained, an increase by more than a factor of two compared with earlier results at 3.35 T of the same system. It was furthermore observed that the addition of gadolinium, which resulted in a twofold polarization increase at 3.35 T, only resulted in a minor improvement at 4.64 T. The dependence of the electron saturation on microwave frequency and microwave power was quantified by first moment measurements which were obtained by nucleus–electron double resonance (NEDOR) experiments. Complete electron saturation was observed for a microwave frequency close to the centre frequency of the ESR line, and by using maximum power of the microwave source. The DNP build-up time at 4.64 T (~3000 s) was prolonged by approximately a factor three over the build-up time at 3.35 T (~1200 s). However, after approximately 20 min of microwave irradiation the polarization at 4.64 T exceeded the polarization at 3.35 T.

1. Introduction

Of the techniques developed for increasing nuclear spin polarization in organic molecules [1–7], Dynamic Nuclear Polarization (DNP) has proved to be one of the most promising. In combination with methods to rapidly dissolve the polarized solid sample it is possible to obtain a solution of molecules containing hyperpolarized nuclei. This has enabled new applications in Nuclear Magnetic Resonance (NMR) spectroscopy as well as medical applications in Magnetic Resonance Imaging (MRI) [6,8–10].

In this work we investigate the DNP enhancement for [1-^{13}C]pyruvic acid, doped with the trityl radical OX063Me, at 4.64 T and 1.15 K. In a previous study at 3.35 T [6] it was observed for the same system that adding small quantities of Gd^{3+} substantially increased the polarization, almost by a factor of two. We show in this work that the polarization obtained at 4.64 T is more than doubled compared with what was obtained at 3.35 T, and furthermore that the addition of Gd^{3+} only has a marginal effect on the polarization at the higher field strength.

2. Theory

2.1. The first moment

The first moment of a spectral line $f(\omega)$ is defined by the integral

$$M_1 = \int_{-\infty}^{\infty} \omega f(\omega) d\omega \tag{1}$$

The shift of the ^{13}C NMR resonance line due to the dipolar fields generated by the presence of the paramagnetic centers, as well as the ^{13}C spins themselves, is given by their respective contributions to the first moment according to [11]

$$\Delta M_1^{IS} = \frac{2}{3}\mu_0 S \xi \gamma_I \gamma_S \hbar N_S P_S \tag{2a}$$

$$\Delta M_1^{II} = \mu_0 I \xi \gamma_I^2 \hbar N_I P_I \tag{2b}$$

Here the first moments are given in rad/s. S and I are the electronic and nuclear spins, respectively, γ_k, N_k, and P_k are the gyro-magnetic ratio, number density, and polarization of spin species k, and the shape factor is given by [11]

$$\xi = \frac{3}{8\pi N_I}\left\langle \sum_i \frac{1 - 3\cos^2\theta_{ij}}{r_{ij}^3} \right\rangle_j \tag{3}$$

One can show that generally the shape factor is bound by $-1/2 \leqslant \xi \leqslant 1$. For the special cases of a sphere, infinitely flat disc and infinitely long cylinder, we have $\xi = 0$, 1, and $-1/2$, respectively. For a cylinder of height h and diameter d, the shape factor only depends on the ratio h/d, and is given by [12]:

$$\xi = \frac{1}{2}(3D_z - 1) \tag{4a}$$

$$D_z = \left(\frac{4}{3\pi} - \int_0^{\infty} \frac{J_1^2(x)}{x^2} e^{-2(h/d)x} dx\right)\frac{d}{h} \tag{4b}$$

* Corresponding author.
E-mail address: haukur.johannesson@ge.com (H. Jóhannesson).

1090-7807/$ - see front matter © 2008 Elsevier Inc. All rights reserved.
doi:10.1016/j.jmr.2008.12.016

where $J_1(x)$ is a first order Bessel function of the first kind. The integral can be evaluated numerically. In Fig. 1 the functional dependence of the shape factor with respect to the h/d ratio is illustrated.

There is also a contribution to the first moment from the proton spins, described by an expression analogous to Eq. (2a), but this will be disregarded in the following since this contribution is effectively constant in all of our experiments.

2.2. Saturating the EPR Line

For the high temperature case when microwaves are applied near the ESR resonance frequency, a rate equation for the electron polarization, taking into account both saturation due to microwaves and spin–lattice relaxation, is given by

$$\frac{dP_S}{dt} = -W \cdot P_S - \frac{1}{T_{1e}}(P_S - P_{0S}) \tag{5}$$

where T_{1e} is the electron spin-lattice relaxation time and $W = \pi\gamma_S^2 B_1^2 g(\Delta)$ is the transition rate due to microwave irradiation, with $g(\Delta)$ being the normalized ESR line at irradiation frequency Δ off resonance, and P_{0S} is the thermal equilibrium polarization. At low temperatures the coupling with the electron non-Zeeman reservoir must also be taken into account. However, for $\Delta = 0$ Eq. (5) is still valid and has the solution

$$P_S(t) = \frac{1}{1 + W \cdot T_{1e}} P_{0S} + \frac{P_{iS}(1 + W \cdot T_{1e}) - P_{0S}}{1 + W \cdot T_{1e}} \times \exp\left\{-\left(W + \frac{1}{T_{1e}}\right)t\right\} \tag{6}$$

where $P_S(0) = P_{iS}$ is the initial electron polarization (not necessarily equal to P_{0S}). The steady state solution is given by

$$P_S^{ss} = \frac{1}{1 + W \cdot T_{1e}} P_{0S} \tag{7}$$

and is approached with a time constant $\tau = (W + \frac{1}{T_{1e}})^{-1}$. By measuring the electron spin relaxation time as well as the saturation time constant, the transition rate W can be determined (*vide infra*).

The power dependence of the electron saturation, and thus the shift in the first moment, can be modeled by using Eqs. (2a) and (7). The shift in the first moment can be written as $\Delta M_1^{IS} = \frac{2}{3}\mu_0 S\xi\gamma_I\gamma_S\hbar N_S P_{0S}(1 - 1/(1 + W \cdot T_{1e}))$. Assuming that the transition rate W is proportional to the applied microwave power, data can be fitted to the simple expression

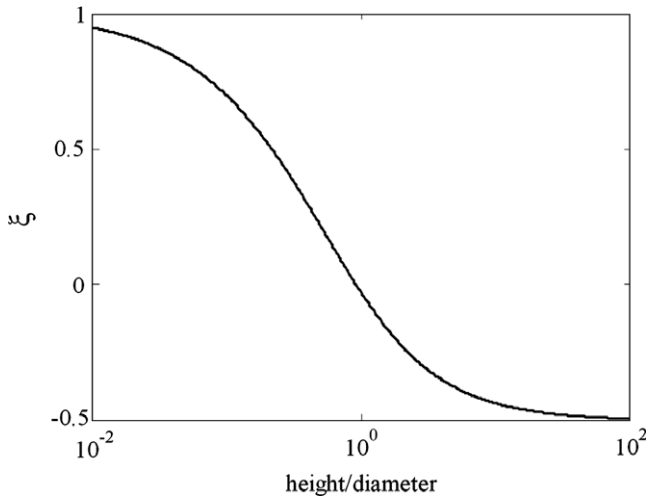

Fig. 1. Semi-logarithmic plot of the shape factor for a cylindrical sample as a function of h/d.

$$A \cdot (1 - 1/(1 + p \cdot B)) \tag{8}$$

where p is the applied power, and B is a constant in units of W^{-1}.

The time dependence of the total shift of the first moment, $\Delta M_1 = \Delta M_1^{IS} + \Delta M_1^{II}$, when performing an electron–nucleus double resonance experiment, was used in order to determine the relaxation time and saturation rate of the electron spins, as well as their residual polarization. The time dependence arises from the manipulations of the nuclear and electron polarizations, by r.f. pulses and microwaves, respectively, and can be described by

$$P_I(t) = P_{0I} e^{-t/\tau_{pulse}} \tag{9a}$$

and

$$P_S(t) = (P_S^{res} - P_{0S})e^{-t/T_{1e}} + P_{0S}, \quad t > 0 \quad \text{(m.w. off)} \tag{9b}$$

where $\tau_{pulse} = -\Delta t/\ln(\cos\alpha)$ is the time constant of the decaying ^{13}C polarization due to the train of r.f. pulses, which are repeated at intervals Δt with a pulse angle α, and P_S^{res} is the residual electron polarization when applying microwaves on resonance.

2.3. The nuclear longitudinal relaxation time

In the limit of fast nuclear spin diffusion, and efficient thermal contact between the electron–electron bath and the nuclear Zeeman bath, the contribution to the nuclear longitudinal relaxation rate from the electron spins is given by [11]

$$\frac{1}{T_{1I}} \approx \left(\frac{\mu_0}{4\pi}\right)^2 \frac{8\pi}{5} \frac{S(S+1)}{3} \frac{N_S\gamma_I^2\gamma_S^2\hbar^2}{b^3} \frac{T_{2e}}{1 + (\omega_I T_{2e})^2}(1 - P_{0S}^2) \tag{10}$$

where b is the radius of the diffusion barrier, ω_I the nuclear resonance frequency, and T_{2e} the electron transverse relaxation time. For a discussion concerning the parameters see [6].

2.4. The electron longitudinal relaxation time

In the solid state the longitudinal electron relaxation is generally assumed to be dominated by the coupling with quantized lattice vibrations, i.e. the phonons. At low enough temperatures the relaxation time is dominated by the one-phonon direct process [13]

$$T_{1e}^{-1} = \frac{3\hbar}{2\pi\rho v^5} \frac{1}{\Delta^2} |V_1|^2 \omega^5 \coth\left(\frac{\hbar\omega}{2k_B T}\right) \tag{11}$$

Two-phonon relaxation processes are expected at higher temperatures, and are given by the Raman process [13]

$$T_{1e}^{-1} = \frac{9}{4\pi^3\rho^2 v^{10}} \left(\frac{k_B T}{\hbar}\right)^7 \left(\frac{\hbar\omega}{\Delta_1}\right)^2 \left\{V_2^2 I_6(\theta_D/T) + \left(\frac{2k_B T}{\hbar\omega}\right)^2 \Delta_1^2 \frac{V_1^4}{\Delta^4} I_8(\theta_D/T)\right\} \tag{12}$$

which is a sum of two contributions, a first-order process of second order perturbation theory, and a second order process of first order perturbation theory. In Eqs. (11) and (12), ρ is the density of the material, v is the speed of sound in the material, Δ is the crystal field splitting, Δ_1 an excited energy state not necessarily equal to Δ, and V_1 and V_2 are the first and second order strains of the electric potential, and θ_D is the Debye temperature. $I_6(\xi)$ and $I_8(\xi)$ are integrals defined by $I_k(\xi) = \int_0^\xi \frac{x^k e^x}{(e^x-1)^2} dx$, which can be evaluated numerically. When $T \ll \theta_D$ the integrals can be approximated by $I_k(\infty) \approx k!$. For low temperatures the direct process gives a $B_0^4 T$ dependence, whereas the two contributions to the Raman process have different field and temperature dependencies, namely $B_0^2 T^7$ and T^9, where the latter term is expected to dominate at temperatures where the direct process is negligible [13].

3. Materials and methods

3.1. The polarizer

The DNP polarizer, based on a standard high resolution, narrow bore, 7 T magnet (Magnex Ltd, Oxford, UK), has been described in detail in Refs. [4–6]. The magnet is charged to 4.64 T, corresponding to a ^{13}C Larmor frequency of 49.7 MHz and an electron $g = 2$ Larmor frequency of 130 GHz. The variable temperature insert (VTI) is cooled by liquid helium that enters through a needle valve from the main helium reservoir, and reaches an operating temperature of 1.1–1.2 K by reducing the vapor pressure through pumping. The stability of the temperature regulation is estimated to be ±50 mK.

The microwave source (ELVA-1 VCOM-06-130-T) has a maximum output power of 60 mW at 130 GHz and a tuning range of 1.2 GHz. The output power can be continuously attenuated by 60 dB.

Apart from the microwave source all equipment is identical to that described in reference [6].

3.2. Sample preparation

The sodium salt of [1-^{13}C]pyruvate was purchased from Cambridge Isotope Laboratories and converted to the acid for subsequent purification by distillation in-house. ^{13}C enrichment is >99% according to the supplier, and the purity should be >99% as determined by ^{1}H NMR. The radical, OX063Me (tris(8-carboxyl-2,2,6,6-tetra(2-(1-methoxy-2,2-d2-ethyl))-benzo[1,2-d:4,5-d']bis(-dithiole-4-yl)methyl sodium salt), was synthesized in-house [14]. The radical has a purity of 92.5% (determined by HPLC), but the impurities are largely believed to also be trityl radicals. The major degradation product of OX063Me is the quinone form, which is not a radical. Under the storage conditions used here, degradation has been observed to be insignificant. Some residual water content is present in the radical, and it is likely that this changes slightly over time from handling. It is estimated that the water content is ~5%. Therefore, an effective radical concentration of 92.5% has been assumed in the sample preparation. $GdCl_3$ was purchased from Sigma Aldrich and was used as received.

The samples were prepared by mixing the required amounts of [1-^{13}C]pyruvic acid and OX063Me, and rapidly dissolving the radical in the solvent. The density of liquid pyruvic acid, 1.26 g/cm^3, was used to calculate the volume of the sample neglecting any (small) volume effect of OX063Me. The concentration of trityl molecules was calculated from the molecular weight with correction for the purity. Samples of four different concentrations of trityl molecules (10, 15, 20 and 50 mmol/L) were used in this study. They will in the following be referred to as samples **1**, **2**, **3** and **4,** respectively. A single sample with the same trityl concentration as sample **2**, but with additional 1.5 mmol/L $GdCl_3$ was used in this study, and is referred to as sample **5**. The samples were stored at −20 °C, and no significant degradation was observed over weeks.

Two versions of sample **2** were prepared with different geometries. One of the samples was a cylindrical sample with $h/d = 6.5 \pm 0.5$ (sample **2a**), and the other one had the shape of a distorted flat disc (sample **2b**). For the remaining samples a similar disc shaped geometry was used as for **2b**. The geometry is an important factor when performing first moment measurements, as it determines the magnitude of the shift and hence the accuracy of the determination of the parameters ΔM_1^{II} and ΔM_1^{IS}. All radical-doped samples were approximately 40 mg in weight, except for sample **2a** (Table 1 gives exact amounts). A single non-doped sample (sample **6**) weighing 200.2 mg was used for determining the thermal equilibrium signal which was used for calculating the polarization of the DNP polarized samples.

3.3. NMR measurements

Solid state NMR data was acquired using a Varian INOVA console (Varian Inc, Palo Alto, CA), connected to the NMR probe described in Ref. [4]. The free induction decay (FID) was obtained using a 7 μs low flip angle r.f. pulse, corresponding to a flip angle of approximately 3.0 ± 0.1°. The number of data points was 1250 and the acquisition time was 1 ms resulting in a spectral resolution of 1000 Hz. The FID data were processed by performing a 1000 Hz exponential apodization and subsequent Fast Fourier Transform (FFT). A linear base line correction and a manual phase correction of 0:th order were employed for the Fourier transformed data. The NMR signal integral was obtained by numerical integration of the absorption line. Flip angle calibration was performed by a fast train of saturating pulses, and the series of signal integrals was fitted to a single exponential function.

For the determination of the thermal equilibrium signal a saturation recovery experiment was performed using an r.f. pulse length of 21 μs (flip angle ~9°) and a repetition time of 3600 s. The signal of the background ^{13}C spins was measured with the same setup and pulse sequence, but without sample.

In order to compare the integrated signal obtained for the thermal equilibrium sample with integrated signals obtained for polarized samples the effect of r.f. pulses was taken into account as described in Appendix A.

Table 1
Obtained parameters for individual samples

Sample	c (mM)[a]	m (mg)	T_{1n} (s)[b]	τ_b (s)[c]	P_l (%)[c]	MW frequency (GHz)[d]	MW Frequency (GHz)[e]	MW Frequency (GHz)[f]	T_{1e} [ms]	ΔM_1^{II} (Hz)	ΔM_1^{IS} (Hz)
1	9.3	40.2	n.d.	5000 ± 600	59 ± 5	130.110	n.d.	n.d.	1090 ± 30	−160 ± 30	347 ± 10
2a	14.1	116.2	n.d.	3500 ± 500	n.d.	130.102	n.d.	n.d.	1040 ± 30	n.d.	−328 ± 10
2b	14.1	41.7	20000 ± 300	3000 ± 600	64 ± 5	130.102	130.164	130.135	1130 ± 30	−200 ± 40	470 ± 15
3	18.5	40.1	21500 ± 500	2500 ± 600	58 ± 5	130.092	130.177	130.138	920 ± 30	−160 ± 30	759 ± 25
4	45.4	39.7	9000 ± 100	475 ± 15	23 ± 5	130.070	n.d.	n.d.	480 ± 20	−50 ± 40	1880 ± 40
5	14.3 1.5[g]	40.0	14000 ± 1000	3000 ± 600	70 ± 5	130.114	130.162	130.138	300 ± 10	−190 ± 40	435 ± 15
6	0	200.2	17000 ± 3000	–	0.104[h]	–	–	–	–	–	–

n.d., not determined.
[a] The trityl radical purity has been taken into account when calculating the concentrations.
[b] Corrected for the effect of r.f. excitations.
[c] Obtained at the frequency for optimum positive DNP enhancements.
[d] Frequency for optimum positive DNP enhancements at 60 mW.
[e] Frequency for optimum negative DNP enhancements at 60 mW.
[f] Frequency for zero crossing of DNP enhancements at 60 mW.
[g] Gadolinium concentration.
[h] Calculated at 4.64 T and 1.15 K.

3.4. DNP vs. microwave frequency

The polarization enhancement as a function of microwave frequency was determined for three of the samples (**2b, 3** and **5**) by different methods. For sample **2b**, two sets of data were obtained using different methods. First the microwave frequency was applied at a value below the EPR resonance frequency, and then stepped up through the resonance in increments of 2 MHz. For each frequency setting, a time of polarization of 800 s was used, and the signal intensity was then measured at the end of each polarization time interval. Subsequently a measurement where the frequency was stepped down was performed, but now the carbon polarization was saturated after each build-up. The measurement on sample **5** was also made using this second method. Since the time used to polarize is short compared with the build-up time, the two methods will be prone to artifacts, especially in the wings where the build-up time is longer. The main purpose of this experiment was however to determine the optimum microwave frequency, which should be well determined despite the mentioned limitations.

For sample **3**, a polarization time of 24000 s was used for every setting of the microwave frequency, and in the case where steady-state had not been reached, an extrapolation to the steady-state value was employed using an exponential fit.

3.5. First moment

The first moment measurements were performed on samples where ^{13}C had been polarized by DNP to the levels given in Table 1. Different types of experiments were performed that used the first moment for extracting relevant parameters. In one type of experiment the optimum microwave frequency for maximum EPR saturation was determined. This was done by monitoring the ^{13}C frequency shift as the microwave frequency was swept through the EPR resonance, allowing an equilibration time of 8–15 s at each frequency step.

The dependence of the electron saturation on the microwave power was also determined for sample **3**, both at the optimum EPR saturation frequency and at a frequency corresponding to optimum DNP. The power level was stepped almost logarithmically, from the lowest power setting to maximum power, in 10 steps, and the change in ^{13}C frequency shift was monitored.

In another type of experiment the electron spin relaxation time T_{1e} and the two contributions to the first moment shifts, ΔM_1^{II} and ΔM_1^{IS}, were determined for the disc shaped samples, and was performed as follows. After ^{13}C polarization by DNP, the microwave frequency was set to the ESR resonance for optimal saturation. After about 10 s, NMR acquisition started with a train of r.f. pulses with a repetition time of 20–30 ms, and after another ~10 s the microwaves were switched off, and the NMR acquisition was continued until the carbon signal was almost completely saturated.

By using the cylindrical sample which has a known shape factor, the residual electron polarization following optimal saturation could be quantified. Since this measurement only needs the ΔM_1^{IS} contribution to the shift a full saturation of the carbon spins was not performed.

The time constant for saturation of the EPR signal could be determined in an analogous fashion to T_{1e}, with the following modification. For a polarized sample, the microwave power was turned off for typically 20 s allowing the electrons to reach thermal equilibrium polarization. The train of r.f. pulses was then initiated and after about 10 s the microwaves were turned on at the optimal saturation frequency.

The first moment measurements described above are based on observing the shift in the nuclear resonance line caused by the electron dipolar field, while performing radio frequency and/or microwave irradiation, and is related to the NEDOR method described in Ref. [11].

Determining the changes in the first moment from the series of acquired spectra is a delicate matter. The changes in the first moment are much smaller than the observed ^{13}C line width of ~7 kHz. It was found that a direct integration of the experimental line shape according to Eq. (1) resulted in unacceptably large errors due to the noise level. A fit to the line shape was then attempted, using Lorentzian as well as Gaussian line shapes. Integration of the fitted line reduces the noise but introduces (as we found small but significant) systematic errors since the line shape is neither Lorentzian nor Gaussian, and furthermore it is not perfectly symmetric. It is important that the behavior in the wings is correctly modeled in the fitting, and the experimental data indicated a decay that seemed to be intermediate between a Lorentzian and a Gaussian. A time domain fitting to a modified Voigt function, as described in Appendix B, was found to give a good representation of the FID and was therefore our method of choice to determine the first moment.

3.6. ^{13}C Longitudinal relaxation time

The longitudinal relaxation time of ^{13}C was measured using DNP polarized samples. The microwaves were switched off, and the decaying ^{13}C magnetization was monitored by measuring the signal intensity with a repetition time of 300–1800 s and a low flip angle r.f. pulse. The signal intensities were corrected for the effect of r.f. pulses, and fitted to an exponential function to give the longitudinal relaxation time.

4. Results

The polarization enhancement as a function of microwave frequency is shown in Fig. 2.The microwave frequencies for maximum positive and negative DNP enhancements for samples **2b**, **3**, and **5** can be found in Table 1 together with the respective zero-crossings of the enhancements. An additional broad peak in the region 129.9–130.0 GHz can be seen for all three samples, albeit only on the low frequency side.

The frequency dependence of the time constant for polarization build-up is shown for sample **3** in Fig. 3. The frequencies corre-

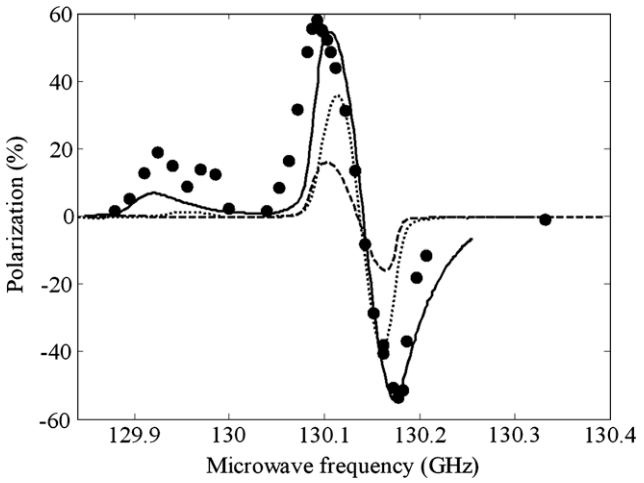

Fig. 2. ^{13}C DNP enhancement as a function of microwave frequency for sample **2b**, determined by two different experiments as described in the text (solid and dashed lines). The purpose was to estimate the optimum mw frequency, and this was achieved without reaching the steady state for any mw frequency. ^{13}C DNP enhancement as a function of microwave frequency for sample **3** (circles), and for sample **5** (dotted line).

sponding to optimum DNP enhancements are marked by vertical dashed lines. In Table 1 the time constants are given for the different samples at the optimum DNP frequency. As can be seen in Fig. 3 the build-up times are fairly constant in a region close to the EPR resonance frequency, but increase dramatically in the wings and are hence less well determined.

The dependence of EPR saturation on microwave power was investigated for sample **3** at frequencies corresponding to optimum DNP enhancement as well as optimum EPR saturation. In Fig. 4 it is seen that the first moment increases rapidly for low microwave power, but reaches a plateau close to the maximum power level used in the other experiments in this study. Fits to Eq. (8) are shown as lines.

In Fig. 5 the variation of the first moment as a function of the microwave frequency for sample **3** can be seen. Two frequency sweeps were performed, one at maximum power (60 mW), and one at 2 mW which gives roughly half of the M_1 value at a microwave frequency corresponding to optimal DNP.

In Fig. 6 the results of the corresponding microwave sweeps, obtained at maximum power, are displayed for samples **1**, **2b**, **4**, and **5**. For samples **1** and **5** a wider frequency region was investigated (Fig. 7). An additional peak is seen for both samples in the region around 129.96 GHz.

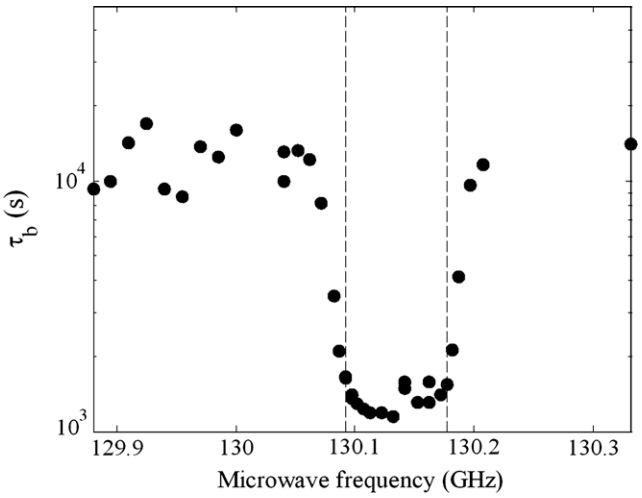

Fig. 3. Time constant for DNP build-up as a function of microwave frequency for sample **3**. The dashed vertical lines indicate the frequencies for optimum DNP enhancements at 130.092 and 130.177 GHz.

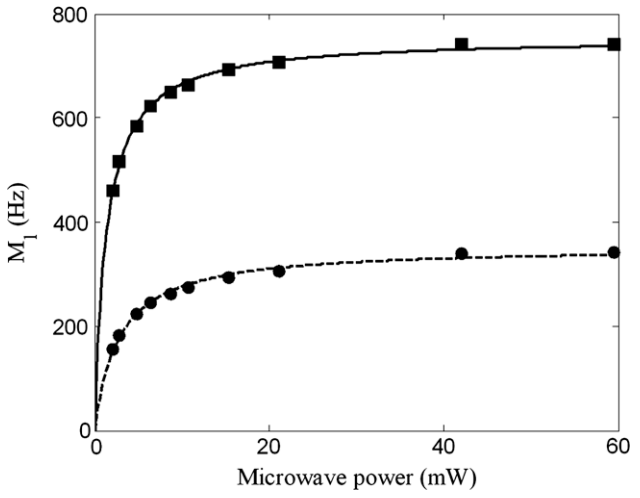

Fig. 4. Power dependence of electron saturation at two microwave frequencies; optimum DNP (circles) and optimum EPR saturation (squares) for sample **3**. The lines are from fits to Eq. (8).

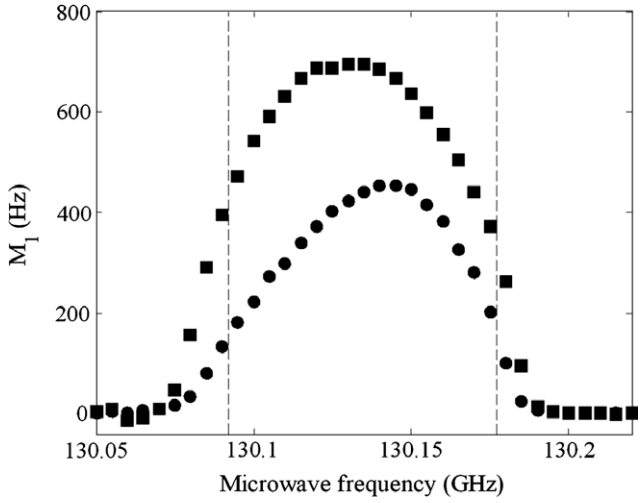

Fig. 5. The degree of electron saturation as a function of microwave frequency for sample **3** using a microwave power of 2 mW (circles) and 60 mW (squares). The dashed vertical lines indicate the frequencies for optimum DNP enhancements at 130.092 and 130.177 GHz. Center of gravity is at 130.134 GHz (circles) and 130.139 GHz (squares).

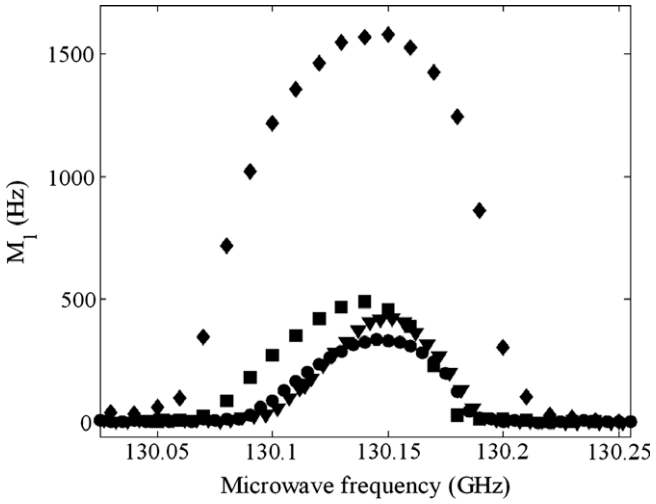

Fig. 6. The degree of electron saturation as function of microwave frequency for samples **1** (circles), **2b** (squares), **4** (diamonds), and **5** (triangles) using a microwave power of 60 mW. Centre of gravity is at 130.146 GHz (**1**), 130.128 (**2b**), 130.143 GHz (**4**), and 130.150 GHz (**5**).

The residual electron polarization after microwave saturation at the optimal saturation frequency was determined by measuring the shift in the first moment for the cylindrical sample (**2a**). After an initial exponential shift due to the electron contribution (ΔM_1^{IS}), a non-exponential, almost linear, decay of the nuclear contribution (ΔM_1^{II}) was observed. This can be attributed to inhomogeneity in the r.f. field arising from the extended geometry of the sample compared with the geometry of the r.f. coil. Due to this only the initial part of the frequency shift was fitted which also is enough to determine the ΔM_1^{IS} contribution. The induced shift in the first moment from the electron spins was found to be equal to -328 ± 10 Hz. The electronic spin lattice relaxation time could also be determined from the time dependence of the frequency shift, and was found to be 1.04 ± 0.03 s.

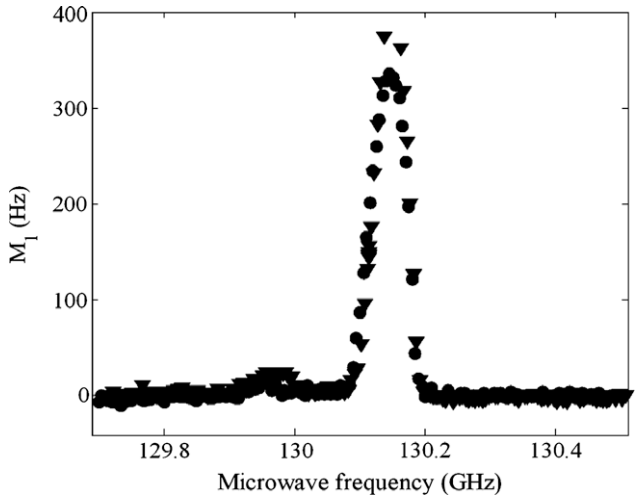

Fig. 7. The degree of electron saturation as a function of microwave frequency for samples **1** (circles) and **5** (triangles). A small extra peak is observed at approximately 129.96 GHz for both samples.

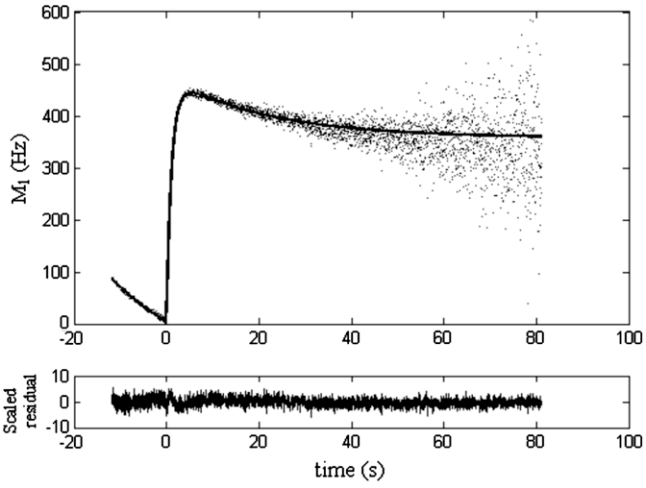

Fig. 8. First moment monitored in a NEDOR experiment for sample **2b** as described in the text. The solid line is from a fit to Eq. (9). The residual shows the difference between the fitted function, and the data points scaled by the inverse signal amplitude. The summed square of the scaled residual was minimized in the fitting procedure.

NEDOR experiments were performed on all samples, and Fig. 8 demonstrates the result of sample **2b**. The data were fitted to Eq. (9) by the standard procedure of minimizing the accumulated squared difference. A weight function proportional to the inverse signal amplitude, was used in the fits. This weight was chosen since it gives a fairly constant residual scatter as can be seen in the same figure. The time constant for the decaying ^{13}C signal can in principle be obtained from the fitting of the first moment data, but a more precise method is to fit the ^{13}C signal integral separately. The fitting of the data to two exponential functions makes it possible to disentangle the two contribution to the shift, ΔM_1^{II} and ΔM_1^{IS}. This means that it is in principle possible to determine the ^{13}C polarization from their ratio by only knowing the concentration ratio N_S/N_I (expected to be the same at all temperatures) and the degree of saturation of the electron spins, without knowing the value of the shape factor. However, due to the increasing scatter of the first moment as the signal intensity decreases, the precision in determining the ΔM_1^{II} contribution is only about 20% which translates to the same precision for the polarization determination. The precision of the ΔM_1^{IS} contribution is on the other hand much higher, about 2–4%, since its time evolution is observed using larger signal intensities giving a better defined first moment. The error in the determination of the electronic relaxation time is also estimated to be 2–4%. In Table 1 the electron spin relaxation times and the respective contributions to the first moments are displayed for the different samples. All NEDOR data in the table were obtained using the time domain fitting described in Section 3.5.

The time constant for the saturation of the EPR signal and the electron relaxation time were measured for sample **2b**, and were found to be 92 ± 5 ms and 1.13 ± 0.03 s, respectively.

The longitudinal ^{13}C relaxation time was measured for samples **2b** and **3**, and was found to be close to 20,000 s for both samples (Table 1). The relaxation time was also measured for a sample without radical (sample **6**), and was found to be slightly shorter, 17000 ± 1000 s. The uncertainty of this measurement is however much larger, not only because of the smaller SNR, but also because the background signal from the sample cup is non-negligible. It was found from the calibration measurements that the relaxation time for the background signal was 10700 ± 700 s, which reduces the total apparent relaxation time of the sample. In order to clearly see the concentration dependence an additional measurement was performed on a sample with the substantially larger radical concentration of 50 mmol/L (sample **4**). For this sample the nuclear relaxation time was 9000 ± 100 s.

The saturation recovery experiment on the non-doped 200.2 mg sample **6** at thermal equilibrium was used for the polarization calibration. The background signal alone was found to be almost half (0.48 ± 0.01) of the thermal equilibrium signal of the sample. The polarization for all samples was calculated from the ratio of the integrated NMR signal to the background signal.

5. Discussion

The dependence of the polarization on the microwave frequency can be seen in Fig. 2. As described in Section 3.4 we chose to perform a complete build-up between successive data points for sample **3**, whereas for the other samples a faster method was used. An asymmetry between the maximum and minimum polarizations can be seen for sample **3**, 58% vs. −54%, which is slightly more pronounced than was observed in our previous study at 3.35 T [6], but the differences are barely significant. It is observed that the microwave frequency corresponding to optimum DNP enhancement is shifted further away from the zero-crossing for the sample with the larger radical concentration. This can be explained by an increase in the EPR line width which is expected to increase with the radical concentration due to electron dipolar interactions. The small extra peak at ∼129.96 GHz seen in Fig. 2 is very close to the expected frequency for the proton solid effect. The proton Larmor frequency is 198 MHz, and using the zero-crossing values in Fig. 2, the two peaks of the solid effect would be expected to appear at frequencies 129.94 GHz and 130.33 GHz. A possible explanation for the appearance of the extra peak is that the protons become polarized when irradiating at this frequency, and a subsequent polarization transfer to ^{13}C occurs. The precise mechanism of this transfer is presently not known, but it could possibly be mediated via the electron non-Zeeman reservoir. However, a strong coupling of the protons to this reservoir is unexpected. We have no explanation why only the low frequency peak is observed.

There is a plateau of minimum build-up time constants close to the EPR resonance frequency (Fig. 3). For frequencies further away from resonance, the time constants increase rapidly when passing the regions corresponding to optimum DNP enhancement. The higher polarization at 4.64 T relative to 3.35 T comes at the price of a longer polarization time. However, already after 20–30 min

the polarization at 4.64 T has exceeded the polarization at 3.35 T, and a higher magnetic field becomes advantageous for ^{13}C DNP with trityl radicals.

The first moment data in Fig. 4 were fitted to Eq. (8) as described in Section 2.2. The fit can be justified on theoretical grounds for data obtained when the microwaves are applied at the EPR resonance, but it seems also be applicable when the microwaves are applied off resonance.

By monitoring the first moment of the ^{13}C signal, a strong dependence of the electron saturation with respect to the microwave frequency was observed. Using the maximum microwave power (60 mW), optimal saturation was found, not surprisingly, close to the EPR resonance frequency, whereas the saturation at the optimal frequency for DNP was found to be reduced by a factor of $\sim$ 1.5–2. In Fig. 5 we see the variation of the first moment as a function of the microwave frequency for sample **3**. It is observed for this sample that at full power the sweep is symmetric with respect to the optimum, whereas for the lower power an asymmetry is observed. This asymmetry reflects the shape of the EPR line [6], and hence this method can be used for indirect EPR detection. The maximum frequency shift when using full microwave power is approximately 700 Hz, and is again obtained at a frequency close the EPR resonance.

The first moment variation with respect to microwave frequency when using maximum microwave power, is displayed in Fig. 6 for all the remaining samples. The width of the saturated region correlates with the radical concentration, which can be attributed to the slightly increasing width of the EPR line. The only exception is the Gd doped sample showing a significantly narrowed region of saturation, and the origin of this behavior is, however, not presently understood.

In Fig. 7, a wider microwave frequency region is investigated for samples **1** and **5**. A shift in the first moment is seen in the same region where the extra peaks in the DNP enhancement of Fig. 2 were observed. This could reflect a change in the proton polarization when hitting this frequency. A change in the proton polarization would also give a change in the first moment of the carbon resonance, which would be described by an equation analogous to Eq. (2a), but with the obvious substitution of parameters.

The optimal saturation of the electron polarization, when applying microwaves at a frequency close to the ESR resonance, can be estimated by comparing the experimentally obtained shift in the first moment for the cylindrical sample with theory. The shape factor for a cylinder with $h/d = 6.5$ is -0.406. Due to the weak dependence of the shape factor for large values of h/d, our conservative error estimate of h/d equal to ±0.5 translates into an error in the shape factor of ±0.007. Using Eq. (2a), the measured frequency shift of -328 ± 10 Hz is consistent with complete electron saturation if we assume an increase in paramagnetic spin density of approximately 15% at 1.15 K compared with room temperature. This reduction in volume upon cooling would also increase the pyruvate density by the same factor, giving a density of 1.45 ± 0.04 g/cm^3. No literature data for the pyruvate density at cryogenic temperatures has been found, but this value is close to the literature value of glycerol, 1.35 g/cm^3 [15]. The shift in the first moment is thus close to what is to be expected, and therefore the conclusion is that we have a complete saturation of the EPR line when irradiating at the optimum microwave frequency.

From the NEDOR experiments a shift in ΔM_1^{IS} of 470 Hz was obtained for sample **2b** (Table 1). Assuming complete EPR saturation one obtains a shape factor, ξ, equal to 0.63. For a cylindrical disc this would correspond to a height to diameter ratio $h/d \sim 0.13$. However in our case the geometry is more complicated, and is expected to vary slightly for the different disc shaped samples. As can be seen in Table 1 ΔM_1^{IS} is roughly proportional to the radical concentration, which is expected from Eq. (2a). The small discrepancy is probably due to slightly different shape factors for the different samples, reflecting their slightly different geometries. Given the large uncertainties in the determination of ΔM_1^{II} there is a reasonable correlation between the nuclear polarization and ΔM_1^{II}, as expected from Eq. (2b).

In the analysis of the first moment data, it has been assumed that the contribution from the proton spins to the first moment of the ^{13}C line is constant. This assumption was validated by observing the effect of r.f. pulses on ^{13}C, with and without microwaves, on the proton NMR signal (data not shown). No effect on the proton polarization was observed, at least on the timescale of the experiment, and it is concluded that the proton contribution to the first moment can be regarded as constant.

From the values of the saturation time constant and electron relaxation time, 92 ms and 1.13 s, respectively, one obtains a transition rate W equal to 10.0 s^{-1}. Inserted into Eq. (7) this would give a steady state polarization equal to 8%, which is in disagreement with the results obtained from sample **2a**. Eq. (5) is however only valid if the spectral diffusion within the ESR line is much faster than the transition rate for a single spin packet. If on the other hand the spectral diffusion is slow the apparent saturation rate of the entire ESR line will be reduced, and in the limit of vanishing spectral diffusion "hole burning" can be achieved. There is, however, no evidence for this limiting case in our experiments, but a reduced transition rate could nevertheless be due to a finite spectral diffusion.

The electron relaxation times for samples **2a** and **2b** were found to be slightly different, which we attribute to different cooling efficiencies for the two sample setups. Compared with data obtained at 3.35 T the field dependence of the electron relaxation time seems to be weak. This observation is not in agreement with the predicted field dependence for the direct process, but is more in line with the field independence of the dominating term in the Raman process. Work by another group has shown that the dominating relaxation mechanism for organic radicals is given by the Raman process, in the range from 100 K down to at least 10 K, which was the lowest temperature explored in their study [16]. In our study it has also been observed that the electron relaxation time depends on the radical concentration. The origin of this dependence could either be due to modification of the parameters that appear in the standard theoretical description, i.e. the phonon

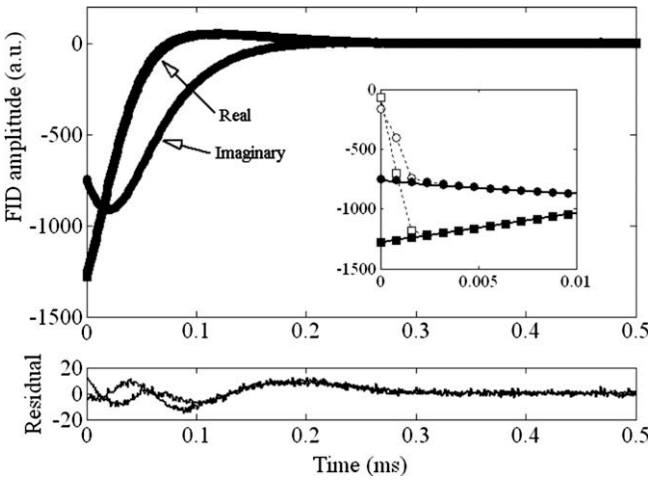

Fig. 9. The initial part of the 1 ms long FID. The squares and circles are the real and imaginary data points, respectively. The residual shows the difference between the data points and the fitted function (modified Voigt as described in the text). The insert shows the initial data points during the first 10 μs, where the initial five corrupted data points (open squares and circles) have been replaced by fitted points as described in Appendix B.

mediated relaxation, or it could be due to dipole-dipole interaction normally neglected in the description of electron relaxation in the solid state. Consequently the reported electron relaxation times (see Table 1) are to be considered apparent values.

The optimum radical concentration with respect to DNP enhancement seems to be similar to what was obtained for the same system in a previous study at 3.35 T [6]. There is a dramatic field dependence regarding the maximum obtainable ^{13}C polarization, which has been more than doubled. Furthermore the addition of a small amount of gadolinium has a modest effect at the field strength in this study, whereas it had a dramatic effect at 3.35 T. We interpret these observations by the presence of a bottleneck at 3.35 T of unknown origin. In the presence of gadolinium or when increasing the field, the bottleneck is removed or at least reduced. This would also explain the marginal effect of adding gadolinium at 4.64 T.

Compared with ^{13}C relaxation data from our work at 3.35 T, the contribution to the nuclear relaxation rate from the radical seems to be about a factor of two larger at 4.64 T. The only parameters that are field dependent in Eq. (10), are b, ω_I, T_{2e}, and P_{0S}. Since the ^{13}C NMR line width is only 3% larger at 4.64 compared with 3.35 T, the diffusion barrier is assumed to be virtually unchanged. The main field dependence arises from ω_I, P_{0S}, and the correlation time, T_{2e}. From this one can deduce that T_{2e} must be about one order of magnitude shorter at 4.64 T compared with 3.35 T.

6. Conclusion

In this study we have demonstrated that increasing the field strength from 3.35 T to 4.64 T has a dramatic increasing effect on the ^{13}C polarization obtained by DNP of [1-^{13}C]pyruvic acid, doped with the trityl radical OX063Me. However, the addition of gadolinium, which was found to be beneficial at 3.35 T, has a marginal effect at 4.64 T. This was attributed to the longer nuclear relaxation time at high field, which is a manifestation of reduced leakage. It was found that optimum polarization was obtained for a trityl radical concentration of approximately 15 mmol/L. For optimized conditions a ^{13}C polarization of 64% was obtained for [1-^{13}C]pyruvic acid at 4.64 T and 1.15 K.

The DNP build-up time at 4.64 T for the optimal radical concentration is roughly 3000 s which is approximately a factor of three longer than the build-up time at 3.35 T (~1200 s). However, after a polarization time of approximately 20 min the polarization at 4.64 T already exceeds the polarization at 3.35 T.

It has been shown that when applying microwaves at the EPR resonance using maximum power of the microwave source, complete saturation is obtained, whereas off-resonance irradiation results in incomplete electron saturation.

The weak dependence of the electron relaxation upon changing the magnetic field strength from 3.35 to 4.64 T is indicative of a dominating Raman process. Furthermore a significant dependence of the electron relaxation on the paramagnetic concentration has been observed.

An enhancement in ^{13}C polarization was observed when applying microwaves at a frequency corresponding to the difference in the electron and the proton Larmor frequencies. This suggests that there is a thermal mixing between the thermal reservoirs of ^{13}C and protons, possibly via the electron dipolar reservoir.

Acknowledgments

The authors would like to acknowledge fruitful discussions with, and contributions from, Dr. Joerg Heckmann, Dr. Gerhard Reicherz, and Prof. Werner Meyer. The magnetic field dependence of the polarization presented in this manuscript has independently been confirmed in their lab.

Appendix A

If we apply excitation pulses corresponding to a flip angle α, with a repetition time T_R, starting at time T_R, we obtain, for a saturation recovery experiment, a sequence of signals where the signal after the n:th pulse is equal to

$$S(n)/S_{te} = \sin\alpha(1 - e^{-T_R/T_1})\frac{1-\cos^n\alpha e^{-nT_R/T_1}}{1-\cos\alpha e^{-T_R/T_1}}$$

here S_{te} is the signal that would be obtained using a single 90° pulse on the sample when it is at thermal equilibrium. The steady state signal is obtained as $n \to \infty$ and is equal to $S^{ss}/S_{te} = \frac{\sin\alpha(1-e^{-T_R/T_1})}{1-\cos\alpha e^{-T_R/T_1}}$. This equation can also be written as $S(t)/S_{te} = A(1 - e^{-t/T_1^{app}})$, where $t = n \cdot T_R$, and T_1^{app} is the apparent, i.e. the measured time constant. The relation between the true relaxation time and the measured one is thus given by $1/T_1 = 1/T_1^{app} + \ln(\cos\alpha)/T_R$. For small flip angles we can use the approximation $\ln(\cos\alpha) \approx -\alpha^2/2$.

For DNP build-up experiments, the signal after the n:th pulse is in a similar way found to be

$$S(n)/S_F = \sin\alpha(1 - e^{-T_R/\tau_{bu}})\frac{1-\cos^n\alpha e^{-nT_R/\tau_{bu}}}{-\cos\alpha e^{-T_R/\tau_{bu}}} + S_{te}/S_F \times \sin\alpha\cos^{n-1}\alpha e^{-nT_R/\tau_{bu}}$$

now S_F is the final signal that would be obtained after a single 90° pulse applied after a complete build-up, and τ_{bu} is the true build-up time. If $S_{te}/S_F \ll 1$ the second term can be omitted. The steady state solution and time dependence are the same as before with the obvious replacements $T_1 \to \tau_{bu}$ and $S_{te} \to S_F$. When comparing the thermal equilibrium signal with polarized signals they should be normalized with the steady state factor $\sin\alpha(1 - e^{-T_R/T_1})/(1 - \cos\alpha e^{-T_R/T_1})$ and $\sin\alpha(1 - e^{-T_R/\tau_{bu}})/(1 - \cos\alpha e^{-T_R/\tau_{bu}})$, respectively (neglecting the second term in the build-up expression).

Appendix B

The experimental data indicated a decay in the wings of the NMR line that seemed to be intermediate between a Lorentzian and a Gaussian line shape. This motivated an attempt of fitting to a Voigt function, which in the frequency domain is the convolution of a Lorentzian and a Gaussian, but in the time domain simply becomes the product $V(t,\tau,\sigma) = L(t,\tau)\cdot G(t,\sigma)$ where $L(t,\tau) = e^{-t/\tau}$ and $G(t,\sigma) = e^{-t^2/\sigma^2}$. Quite generally the FID can be written as a product of a complex exponential and a decaying envelope function as $\Phi(t) = \exp(ih(t))\cdot g(t)$. Quadrature detection of the FID enables separate detections of the real and imaginary parts $\Phi_{Re}(t)$ and $\Phi_{Im}(t)$ and hence the modulus $|\Phi(t)| = (\Phi_{Re}^2(t) + \Phi_{Im}^2(t))^{1/2}$ which is identical to the envelope function $g(t)$. Before fitting the FID, five initial points were deleted ("left shift") since they were corrupted due to the transient recovery of the receiver. However, deletion of initial points led to the observation that the obtained change in first moment increased linearly with the number of deleted points beyond the corrupted ones. This motivated an extrapolation of the FID to $t = 0$, i.e. a replacement of the corrupted points with fitted ones. This was accomplished by fitting the initial non-corrupted 25 data points to a second order polynomial. An alternative procedure of determining the first moment after a sequence of increasing left shifts without extrapolating the FID was also performed. A linear fit of the first moments with a subsequent extrapolation to zero left shifts produced the same result as the first method. The first method was chosen since it was less time consuming. The fitting of the total FID was then done in two steps, first the envelope function was determined, and second the frequency part was determined using the previously obtained envelope function. The fit of the envelope using the Voigt function resulted in a small

oscillating decaying residual which motivated a modification to the Voigt function by multiplying it with $r(t) = 1 - a \cdot \sin(\varepsilon t)$. In the frequency domain this small correction adds a symmetric broadening around $\pm\delta$ from the base line up to a height which is determined by the parameter a. No physical justification is found for this modified Voigt function. However this is not necessary since only a good representation of the line shape is sought. For the series of FIDs obtained from the train of r.f. pulses a fit of the envelope to the function $g(t) = A \cdot L(t,\tau) \cdot G(t,\sigma) \cdot r(t) + c_{dc}$ was performed. The constant c_{dc} represents a dc off-set which is introduced by taking the modulus since the noise now is only positive (this constant is however removed in the fitting of the frequency part). After a fit of all parameters to the first FID, the parameters a and δ were then fixed for the remaining envelopes. Fitting of the frequency part, $\exp(ih(t))$, showed that a linear function $h(t)$ (phase and frequency) did not accurately represent the data. This is however to be expected since the line shape is not symmetric. The Fourier transform of a FID with a linear $h(t)$ will always give a symmetric line shape regardless of the envelope function. This follows from the definition of the Fourier transform together with the time symmetry of the envelope function. Introducing higher order terms in $h(t)$ decreases the error of the fit, but also increases the number of parameters to be fitted making the procedure more time consuming. We found that including a second order term was sufficient to reduce the fitting error almost to the level of the noise. Since the phase drift was found to be negligible, the constant part of $h(t)$ was determined from a fit to the first FID, and was then fixed for the fits of the remaining FIDs. If the spectral line shape would have been symmetric, and $h(t)$ a linear function, the first moment would have been identical to the coefficient for the term linear in $h(t)$. For our case it is not that simple, so the first moment was calculated in the frequency domain by Fourier transforming the fitted FIDs and integrating according to Eq. (1). A fourfold zero filling was employed before Fourier transforming the FID, and the integration was performed by a numerical Simpson integration method. Fig. 9 shows a fit of the first FID for sample **2b**.

References

[1] H. Jóhannesson, O. Axelsson, M. Karlsson, Transfer of para-hydrogen spin order into polarization by diabatic field cycling, C.R. Physique 5/3 (2004) 315–324.
[2] M. Goldman, H. Jóhannesson, Conversion of a proton pair para order into 13C polarization by rf irradiation, for use in MRI, C.R. Physique 6/4-5 (2005) 575–81.
[3] PCT publication WO 1999/35508 priority date 5 January 1998.
[4] J.H. Ardenkjaer-Larsen, B. Fridlund, A. Gram, G. Hansson, L. Hansson, M.H. Lerche, R. Servin, M. Thanning, K. Golman, Increase in signal-to-noise ratio of >10, 000 times in liquid-state NMR, Proc. Natl. Acad. Sci. USA 100 (18) (2003) 10158–10163.
[5] J. Wolber, F. Ellner, B. Fridlund, A. Gram, H. Jóhannesson, G. Hansson, L. Hansson, M.H. Lerche, S. Mansson, R. Servin, M. Thaning, K. Golman, J.H. Ardenkjaer-Larsen, Generating highly polarized nuclear spins in solution using dynamic nuclear polarization, Nucl. Instr. Meth. Phys. Res. A 526 (2004) 173–181.
[6] J.H. Ardenkjaer-Larsen, S. Macholl, H. Jóhannesson, Dynamic nuclear polarization with Trityls at 1.2 K, Appl. Magn. Reson. 34 (2008) 509–522.
[7] K. Golman, O. Axelsson, H. Jóhannesson, S. Månsson, C. Olofsson, S.J. Petersson, Parahydrogen-induced polarization in imaging: subsecond 13C angiography, Magn. Reson. Med. 46 (2001) 1–5.
[8] K. Golman, J.H. Ardenkjaer-Larsen, J.S. Petersson, S. Mansson, I. Leunbach, Molecular imaging with endogenous substances, Proc. Natl. Acad. Sci. USA 100 (18) (2003) 10435–10439.
[9] K. Golman, R. in't Zandt, M. Thaning, Real-time metabolic imaging, Proc. Natl. Acad. Sci. USA 103 (2006) 11270–11275.
[10] K. Golman, R. in't Zandt, M.H. Lerche, R. Pehrson, J.H. Ardenkjaer-Larsen, Metabolic imaging by hyperpolarized 13C magnetic resonance imaging for in vivo tumor diagnosis, Cancer Res. 66 (2006) 10855–10860.
[11] A. Abragam, M. Goldman, Nuclear Magnetism: Order and Disorder, Clarendon Press, Oxford, 1982.
[12] G.W. Crabtree, Demagnetizing fields in the de Haas-van Alphen effect, Phys. Rev. B 16 (1977) 1117–1125.
[13] A. Abragam, B. Bleaney, EPR of Transition Ions, Clarendon Press, Oxford, 1970.
[14] PCT publication WO 2006/011811, priority date 30 July 2004.
[15] E. Koivula, M. Punkkinen, W.H. Tanttila, E.E. Ylinen, Dynamics of proton spin-lattice relaxation in glycerol, Phys. Rev. B 32 (1985) 4556–4564.
[16] J.R. Harbridge, S.S. Eaton, G.R. Eaton, Electron spin–lattice relaxation processes of radicals in irradiated crystalline organic compounds, J. Phys. Chem. A 107 (2003) 598–610.